FLEXURAL ANALYSIS OF LAMINATED PLATE EMBEDDED ON ELASTIC MEDIUM FOUNDATION SUBJECTED TO TRANSVERSE LOAD USED IN INDUSTRIES: A RADIAL BASIS FUNCTION APPROACH

Chandan Kumar[1], Appaso M Gadade[2], Rahul Kumar[3], Harish K. Sharma[4] and Jeeoot Singh[5]

[1]Department of Mechanical Engineering, BIT, Mesra Patna Campus, India

[2]Thapar Institute of Engineering and Technology, Patiala 147004 India.

[3]Department of mechanical engineering DDU, Gorakhpur, India

[4]Department of Mechanical Engineering, GLA University, Mathura, India

[5]Department of Mechanical Engineering, MMMUT, Gorakhpur, India

Corresponding Author: rahul22mech@gmail.com

Abstract: *The present study developed the radial basis functions based meshless collocation technique (RBFMCT) using equivalent five variables higher order shear deformation theory (HSDT) for the static analysis of elastically supported laminated plates. The RBFMCT is based on strong form formulation which is suitable to examine for the laminated plates embedded on elastic medium foundation subjected to transverse load used in industries. The governing differential equation for laminated plates embedded on elastic medium foundation is formulated via Hamilton's principle. Here, seventeen different types of RBFs are taken to demonstrate the correctness and consistent of the present solution methodology regarding nodes number and computational time. In addition, the effects of I, L and T types of transverse loading, span to thickness ratio, aspect ratio, effect of RBFs, effect of two parameters elastic foundation on the flexural responses of the laminated plate is also investigated in detail.*

Keywords*: Flexural analysis, Laminated plate, Elastic foundation, Radial basis function, Transverse loading, Meshfree Technique.*

1. Introduction

Plates/panels are one of the important structural elements in aerospace, automotive, marine and other high performance engineering structures. During their service life they are subjected to

different loading conditions and resulting deformations may be moderate to large. These structural components are preferably made up of fiber reinforced composites stacked in layers or sandwich structures resulting in saving of weight. There are several plate models that intend to predict the kinematics of those structures more precisely and more effectively. Pagano [1] originated a pioneering work by adducing an exact 3-D elasticity solution for the bending response of laminated cylinders. In extension to the above work, Pagano [2] presented a 3D elasticity solution for the bending analysis of rectangular laminates plate. Srinivas and Rao [3] introduced a 3D linear elasticity solution for the structural response of simply supported thick laminated plates with nine elastic constants of orthotropy. Reddy et al. [4] carried out finite element analyses to study the bending response of laminated plates. Savithri and Varadan, [5] investigated an authentic static response of laminated orthotropic plates. Sahoo et al. [6] investigated the bending and the natural frequency response of laminated woven glass/epoxy plate via two HSDT model. Karama et al. [7] introduced new HSDT displacement model for the flexural analysis of laminated plate. Paydar and Libove, [8] introduced a finite-difference formulation for a small deflection theory be associated with GDEs and a total potential energy formulation for studying flexural elastic sandwich plates. Saood et al. [9] studied the effects of fiber angle on steady-state response of laminated plates. Khan and Saxena [10] reviewed the mechanical properties of polymer composite under different loading rates. Rodrigues et al. [11] introduced meshless method to examine the flexural analysis of antisymmetric angle-ply laminates via distinct HSDTs displacement model. Chai et al.[12] examined the bending analysis of laminated columns under uniaxial compression and transverse load via closed-form formulation. Ferreira et al.[13] presented collocation with a Deslaurier Dubuc interpolating basis for the flexural and free vibrations analysis of isotropic and laminated plates in the framework of FSDT displacement model. Pavan and Nanjunda Rao [14] used Isogeometric collocation approach for the linear bending analysis of laminated plates via Reissner–Mindlin theory. Xiao et al.[15] used meshless technique for the bending study of thick laminated composite elastic plates. Ray [16] investigated the 3D exact solutions for the flexural response of antisymmetric angle ply laminated plates governed by FSDT displacement model. The MQRBF method [17] is the most valuable and implemented in various applications. Basically, Hardy proposed the MQRBF for data surface fitting [18] and Kansa used for calculating the partial differential equations [19]. Ferreira expanded the MQRBF to analyses beams, plates, and shells [20] ,[21], [27].Recently Kumar and Singh [24] implemented MQRBF for the analysis of plates. Tornabene [25] used RBFs approach for the analysis of laminated shells and panels. Xiang and Kang [26] implemented thin-plate-spline RBF for the analysis of laminated plate. Liew et al. [27]

introduced a review on the enhancement of element-free or meshfree methods and their applications for laminated and FGM structures analysis.

In the current work, the flexural analysis of elastically supported laminated plate under *I, L* and *T* shape of transverse loading is considered under the framework of HSDT model. From the author's knowledge, the various type of loading used in industries is considered for elastically supported laminated plate, which is not available in the literature. Parametric studies are directed to study the flexural response and the influence of various influential factors (e.g., elastic foundation, various types of transverse loading, aspect ratio, span to thickness ratio, and orthotropy ratio,) is evaluated.

2. Mathematical Formulation

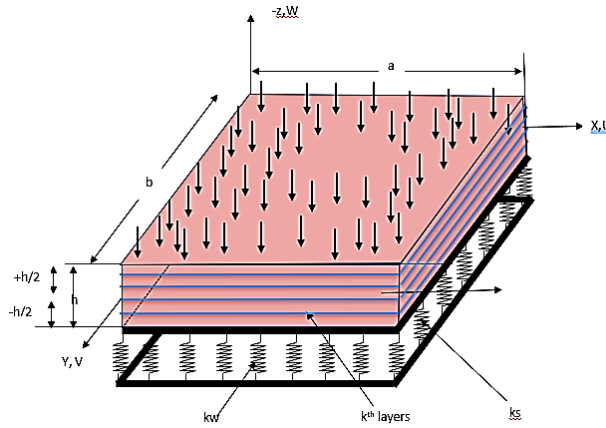The laminated plate with length, breadth and thickness are '*a*','*b*', and '*h*' which is shown in Figure.1.

Fig. 1. Laminated plate

The displacement field with the HSDT model is formulated as :

$$U = u_0(x,y) - z\frac{\partial w_0(x,y)}{\partial x} + f(z)\,\phi_x(x,y)$$

$$V = v_0(x,y) - z\frac{\partial w_0(x,y)}{\partial y} + f(z)\phi_y(x,y) \tag{1}$$

$$W = w_0(x,y)$$

where u_0, v_0 and w_0 are midplane displacements and ϕ_x, ϕ_y are rotations of the normal to the midplane due to shear deformation about y and x-axes, respectively, $\sin\left(\dfrac{2\pi z}{h}\right) - \dfrac{2\pi z}{h}\cos(\pi)$ is transverse shear stress function proposed by [28],

The strain displacements relations are formulated as:

$$
\begin{Bmatrix} \varepsilon_{xx} \\ \varepsilon_{yy} \\ \gamma_{xy} \\ \gamma_{yz} \\ \gamma_{zx} \end{Bmatrix} = \begin{Bmatrix} \dfrac{\partial u_0}{\partial x} - z\dfrac{\partial^2 w_0}{\partial x^2} + g(z)\dfrac{\partial \phi_x}{\partial x} \\[2mm] \dfrac{\partial v_0}{\partial y} - z\dfrac{\partial^2 w_0}{\partial y^2} + g(z)\dfrac{\partial \phi_y}{\partial y} \\[2mm] \dfrac{\partial u_0}{\partial y} + \dfrac{\partial v_0}{\partial x} - 2z\dfrac{\partial^2 w_0}{\partial x \partial y} + g(z)\dfrac{\partial \phi_x}{\partial y} + g(z)\dfrac{\partial \phi_y}{\partial x} \\[2mm] \dfrac{\partial g(z)}{\partial z}\phi_y \\[2mm] \dfrac{\partial g(z)}{\partial z}\phi_x \end{Bmatrix}
\tag{2}
$$

The stress-strain relations for k^{th} layer of the laminated plate is formulated as[29],:

$$
\begin{Bmatrix} \sigma_{xx} \\ \sigma_{yy} \\ \sigma_{xy} \\ \sigma_{yz} \\ \sigma_{zx} \end{Bmatrix}_k = \begin{bmatrix} \overline{Q}_{11} & \overline{Q}_{12} & \overline{Q}_{16} & 0 & 0 \\ \overline{Q}_{12} & \overline{Q}_{22} & \overline{Q}_{26} & 0 & 0 \\ \overline{Q}_{16} & \overline{Q}_{26} & \overline{Q}_{66} & 0 & 0 \\ 0 & 0 & 0 & \overline{Q}_{44} & \overline{Q}_{45} \\ 0 & 0 & 0 & \overline{Q}_{45} & \overline{Q}_{55} \end{bmatrix}_k \begin{Bmatrix} \varepsilon_{xx} \\ \varepsilon_{yy} \\ \gamma_{xy} \\ \gamma_{yz} \\ \gamma_{zx} \end{Bmatrix}_k
\tag{3}
$$

The Hamilton's principle of the laminated plate is written as.

$$
\int_{t_1}^{t_2} \delta(UE + UEF - KE)\, dt = 0
\tag{4}
$$

where KE = Kinetic energy, UE = Strain energy, UEF= strain energy of the elastic foundation

The UE of the elastically supported laminated plate is formulated as [30]

$$
UE = \frac{1}{2}\int_{-\frac{h}{2}}^{\frac{h}{2}} \int_A (\sigma_{xx}\varepsilon_{xx} + \sigma_{yy}\varepsilon_{yy} + \sigma_{xy}\gamma_{xy} + \sigma_{yz}\gamma_{yz} + \sigma_{xz}\gamma_{xz})\, dz\, dA
\tag{5}
$$

The UEF of the elastically supported laminated plate is formulated as [31]

$$
UEF = \frac{1}{2}\left(\int_A kw(w_0{}^2) - ks\left(\left(\frac{\partial w_0}{\partial x}\right)^2 + \left(\frac{\partial w_0}{\partial y}\right)^2 \right) dA \right)
\tag{6}
$$

The potential energy due to transverse loads of the elastically supported laminated plate is formulated as

$$VE_q = \int_A F_z \, w \, dA \tag{7}$$

where F_z is transverse pressure.

The *GDEs* of the plate are achieved by cumulating the coefficients of δu_0, δv_0, δw_0, $\delta\phi_x$ and $\delta\phi_y$ can be formulated as:

$$\delta u_0 : \quad \frac{\partial N_x}{\partial x} + \frac{\partial N_{xy}}{\partial y} = 0$$

$$\delta v_0 : \quad \frac{\partial N_{xy}}{\partial x} + \frac{\partial N_y}{\partial y} = 0$$

$$\delta w_0 : \quad \frac{\partial^2 M_x}{\partial x^2} + \frac{\partial^2 M_y}{\partial y^2} + 2\frac{\partial^2 M_{xy}}{\partial x \partial y} - kw(w_0) + ks\left(\frac{\partial^2 w_0}{\partial x^2} + \frac{\partial^2 w_0}{\partial y^2}\right) = F_z \tag{8}$$

$$\delta\phi_x : \quad \frac{\partial M_x^f}{\partial x} + \frac{\partial M_{xy}^f}{\partial y} - Q_x^f = 0$$

$$\delta\phi_y : \quad \frac{\partial M_{xy}^f}{\partial x} + \frac{\partial M_y^f}{\partial y} - Q_y^f = 0$$

The force and moment resultants used in Eq. (8) are formulated as:

$$N_{ij}, M_{ij}, M_{ij}^f = \int_{-h/2}^{+h/2} (\sigma_{ij}, z\sigma_{ij}, g(z)\sigma_{ij}) \, dz$$

$$Q_x^f, Q_y^f = \int_{-h/2}^{+h/2} (\sigma_{xz}, \sigma_{yz})\left(\frac{\partial g(z)}{\partial z}\right) dz \tag{9}$$

The plate stiffness coefficients of laminated plate are written as

$$A_{ij}, B_{ij}, D_{ij}, E_{ij}, F_{ij}, H_{ij} = \sum_{k=1}^{n} \int_{z_k}^{z_{k+1}} \overline{Q}_{ij}\left(1, z, z^2, f(z), z\,f(z), f^2(z)\right) dz \ , \ i, j = 1, 2, 6 \tag{10}$$

$$(A_{ij} = \sum_{k=1}^{n} \int_{z_k}^{z_{k+1}} \overline{Q}_{ij}\left(\frac{\partial f(z)}{\partial z}\right)^2 dz \qquad\qquad i, j = 4, 5 \tag{11}$$

Simply supported (SSSS) boundary condition is consider as:

$$x = 0 \ \ and \ \ a : \ N_{xx} = 0, \ v_0 = 0, \ w_0 = 0, \ M_{xx} = 0, \ \phi_y = 0 \tag{12}$$

$$y = 0 \ and \ b: u_0 = 0, \ N_{yy} = 0, \ w_0 = 0, \ \phi_x = 0, \ M_{yy} = 0 \qquad (13)$$

3. Solution Methodology

The importance of *RBF*-based meshfree methods is that it discretizes the *GDEs* directly and produce a high rate of convergence with good accuracy. In the present analysis, we have considered nodes distribution uniformly for a 2-D rectangular domain having *IN* interior nodes, BN boundary nodes, and *N* is the total nodes which are the sum of *IN* and *BN* which is shown in [32]. Here, we have considered seventeen types of RBFs that are used in various types of computational engineering applications and listed in Table 1. The GDEs with five unknown variables u_0, v_0, w_0, ϕ_x and ϕ_y can be an interpolation in the form of the radial distance between

nodes. The radial distance r as $r = \|X - X_j\| = \sqrt{\left(\dfrac{x - x_j}{a}\right)^2 + \left(\dfrac{y - y_j}{b}\right)^2}$ for plate where *a* and *b* are the

length and breadth of a rectangular plate.

Table 1. Different type of RBFs applied in computation applications.

S.No	RBF	S.No	RBF
1	Polynomial, g1 r^k	10	Hardy's Multiquadric, g10 $\sqrt{(k^2 + r^2)}$
2	Gaussian quadratic, g2 $e^{(-k^2 r^2)}$	11	Hardy's Inverse Quadric g11 $(k^2 + r^2)^{-1}$
3	Thin Plate Spline, g3 $\log(r) r^{2k}$	12	Multi-quadratic, g12 $\sqrt{1 + (kr)^2}$
4	Wendland's C2, g4 $(1-kr)^4 (4kr+1)$	13	Inverse Multi-quadratic, g13 $\left(\sqrt{1+(kr)^2}\right)^{-1}$
5	Wendland's C4, g5 $(1-kr)^6\left(\left(35(kr)^2\right)+(18kr)+3\right)$	14	Generalized Inverse Multi-quadratic, g14 $\left(1+(kr)^2\right)^{-2}$
6	Wendland's C6, g6 $(1-kr)^8\left(\left(32(kr)^3\right)+\left(25(kr)^2\right)+(8kr)+1\right)$	15	Inverse quadratic, g15 $\left(1+(kr)^2\right)^{-1}$
7	Hyperbolic secant, g7 $\sec h\left(k\sqrt{r}\right)$	16	Multi-quadratic Shu II, g16 $\sqrt{r^2 + k}$
8	Wu-C2, g8 $(1-kr)^5\left(8+40kr+48(kr)^2+25(kr)^3+5(kr)^4\right)$	17	Inverse Multi-quadratics, g17 $\left(\sqrt{r^2+k}\right)^{-1}$
9	Wu-C4, g9 $(1-kr)^6\left(6+36kr+82(kr)^2+72(kr)^3+30(kr)^4+5(kr)^5\right)$		

where 'k' is the shape parameter that is responsible for accurate numerical solution and stability of the method in the computational domain. It is additionally reported that stability and accuracy both simultaneously cannot be ensured.

The variable u can be interpolated in form of radial distance between nodes. The solution of the *GDEs* (8) is assumed in terms of *RBFs* for nodes 1: N, as;

$$u_0 = \sum_{j=1}^{N} \alpha_j^{u_0} g\left(\left\|X - X_j\right\|, k\right) \tag{14}$$

$$v_0 = \sum_{j=1}^{N} \alpha_j^{v_0} g\left(\left\|X - X_j\right\|, k\right) \tag{15}$$

$$w_0 = \sum_{j=1}^{N} \alpha_j^{w_0} g\left(\left\|X - X_j\right\|, k\right) \tag{16}$$

$$\phi_x = \sum_{j=1}^{N} \alpha_j^{\phi_x} g\left(\left\|X - X_j\right\|, k\right) \tag{17}$$

$$\phi_y = \sum_{j=1}^{N} \alpha_j^{\phi_y} g\left(\left\|X - X_j\right\|, k\right) \tag{18}$$

where, N is total numbers of nodes.

The *GDEs* are discretized and formulated in compact matrix form as:

$$\left(\begin{bmatrix} [K]_I \\ [K]_B \end{bmatrix}_{5N \times 5N} + \begin{bmatrix} [K_I]_F \\ [K_B]_F \end{bmatrix}\right) \{\delta\}_{5N \times 1} = \begin{Bmatrix} [F]_L \\ 0 \end{Bmatrix}_{5N \times 1} \tag{19}$$

$$\{\delta\} = \left(\begin{bmatrix} [K]_I \\ [K]_B \end{bmatrix} + \begin{bmatrix} [K_I]_F \\ [K_B]_F \end{bmatrix}\right)^{-1} \begin{Bmatrix} [F]_L \\ 0 \end{Bmatrix} \tag{20}$$

where,

$$[K]_I = \begin{bmatrix}
[K^l_{1u}]_{(NI,N)} & [K^l_{1v}]_{(NI,N)} & [K^l_{1w}]_{(NI,N)} & [K^l_{1\phi_x}]_{(NI,N)} & [K^l_{1\phi_y}]_{(NI,N)} \\
[K^l_{2u}]_{(NI,N)} & [K^l_{2v}]_{(NI,N)} & [K^l_{2w}]_{(NI,N)} & [K^l_{2\phi_x}]_{(NI,N)} & [K^l_{2\phi_y}]_{(NI,N)} \\
[K^l_{3u}]_{(NI,N)} & [K^l_{3v}]_{(NI,N)} & [K^l_{3w}]_{(NI,N)} & [K^l_{3\phi_x}]_{(NI,N)} & [K^l_{3\phi_y}]_{(NI,N)} \\
[K^l_{4u}]_{(NI,N)} & [K^l_{4v}]_{(NI,N)} & [K^l_{4w}]_{(NI,N)} & [K^l_{4\phi_x}]_{(NI,N)} & [K^l_{4\phi_y}]_{(NI,N)} \\
[K^l_{5u}]_{(NI,N)} & [K^l_{5v}]_{(NI,N)} & [K^l_{5w}]_{(NI,N)} & [K^l_{5\phi_x}]_{(NI,N)} & [K^l_{5\phi_y}]_{(NI,N)}
\end{bmatrix}_{(5NI \times 5N)} \tag{21}$$

$$[F]_L = \begin{Bmatrix} 0 \\ 0 \\ q \\ 0 \\ 0 \end{Bmatrix}_{5N \times 1} \tag{22}$$

$$[K_I]_F = \begin{bmatrix}
[0] & [0] & [0] & [0] & [0] \\
[0] & [0] & [0] & [0] & [0] \\
[0] & [0] & \left[K_w w_0 - K_s\left(\dfrac{\partial^2 w_0}{\partial x^2} + \dfrac{\partial^2 w_0}{\partial y^2}\right)\right] & [0] & [0] \\
[0] & [0] & [0] & [0] & [0] \\
[0] & [0] & [0] & [0] & [0]
\end{bmatrix}_{(5 \times NI, 5 \times N)} \tag{23}$$

$$[K_B]_F = [0]_{(5 \times NB, 5 \times N)} \tag{24}$$

4. Results and Discussions

The flexural response of elastically supported laminated plates under *I*, *L*, and *T* type transverse loading is investigated in this section. Numerous cases have been examined to show the efficacy and applicability of the present formulation. After convergence study, 15×15 nodes are used throughout the study. Following material properties are taken throughout the analysis except variation of E_1/E_2, where E_1 is varied. $E_1 = 25 E_2$; $G_{12} = G_{13} = 0.5 E_2$; $G_{23} = 0.2 E_2$; $v_{12} = 0.25$. The non-dimensionalized deflection and stresses are expressed as:

$$\bar{w}_c = \left(\frac{100h^3 E_2}{q_0 a^4}\right) w\left(\frac{a}{2},\frac{a}{2},0\right), \bar{w}_m = \left(\frac{100h^3 E_2}{q_0 a^4}\right) w_m, \bar{\sigma}_{xx} = \frac{h^2}{q_0 a^2}\sigma_{xx}\left(\frac{a}{2},\frac{a}{2},\frac{h}{4}\right), \bar{\sigma}_{yy} = \frac{h^2}{q_0 a^2}\sigma_{yy}\left(\frac{a}{2},\frac{a}{2},\frac{h}{4}\right)$$

$$\bar{\sigma}_{xy} = \frac{h^2}{q_0 a^2}\sigma_{xy}\left(0,0,\frac{h}{2}\right), \bar{\sigma}_{yz} = \frac{h}{q_0 a}\sigma_{yz}\left(\frac{a}{2},0,0\right), \bar{\sigma}_{xz} = \frac{h}{q_0 a}\sigma_{xz}\left(0,\frac{b}{2},0\right)$$

where w_c is central deflection and w_m is maximum deflection. q for different types of loading conditions shown in Figure 2.

| L loading | I loading | T loading |
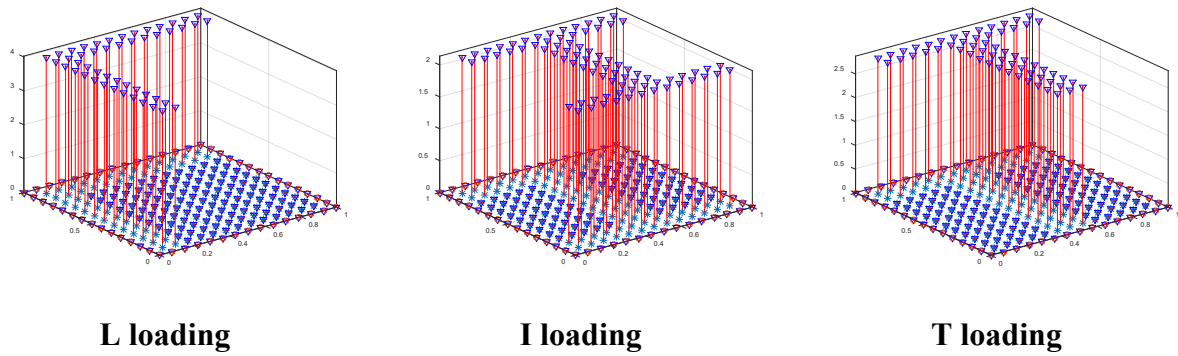
Fig. 2. Various types of loads used in industries.

4.1. Convergence and validation study

Table 2 represents the convergence study of normalized central deflection of laminated plate. It is observed that the present solution obtained by the seventeen RBFs are converged well and also in good agreement with the result presented in the literature by 3D Quasis solution [33] and 2D HSDT solution by Reddy [34]. It can also be noted that all the RBFs produced good results, and the convergence rate is less than 2% after 13×13 nodes.

Table 2. Convergence study of normalized central deflections for laminated plate using several basis functions.

RBFs	9×9	11×11	13×13	15×15	17×17	3D Ref.[33]	Reddy [34]
g1	0.6404	0.7348	0.7167	0.721	0.717	0.7282	0.7147
g2	0.7196	0.7196	0.7195	0.7195	0.7195	0.7282	0.7147
g3	0.4484	0.688	0.7139	0.7179	0.7189	0.7282	0.7147

g4	0.6842	0.6842	0.7167	0.721	0.717	0.7282	0.7147
g5	0.7444	0.7321	0.7271	0.7251	0.7202	0.7282	0.7147
g6	0.7146	0.7162	0.7177	0.7186	0.7192	0.7282	0.7147
g7	0.7132	0.7212	0.7172	0.7175	0.7187	0.7282	0.7147
g8	0.7284	0.7264	0.7234	0.7212	0.7204	0.7282	0.7147
g9	0.5672	0.7059	0.7167	0.7186	0.7192	0.7282	0.7147
g10	0.7076	0.7129	0.7153	0.7167	0.7175	0.7282	0.7147
g11	0.7041	0.7107	0.7138	0.7155	0.7165	0.7282	0.7147
g12	0.6734	0.701	0.7107	0.7154	0.7175	0.7282	0.7147
g13	0.6662	0.7003	0.7181	0.7161	0.7181	0.7282	0.7147
g14	0.6237	0.6887	0.7044	0.7124	0.7162	0.7282	0.7147
g15	0.6476	0.6941	0.7078	0.7143	0.7172	0.7282	0.7147
g16	0.7126	0.7167	0.7185	0.7194	0.7172	0.7282	0.7147
g17	0.708	0.7143	0.7169	0.7181	0.7187	0.7282	0.7147

Figure 3 shows the convergence study of $\bar{\sigma}_{xx}$ for a laminated plate for seventeen RBFs. It is noticed that all the RBFs predict less than 2 % after 13×13 nodes and show good agreement with 3D Quasis solution and 2D HSDT solution. So, based on the convergence study, a 15×15 node is used throughout the study. Figure 4 shows the comparison central deflections for a laminated plate for different RBFs and computational time required. The results shows that the RBF g9 requires more time for computation of central deflections followed by RBF g8.
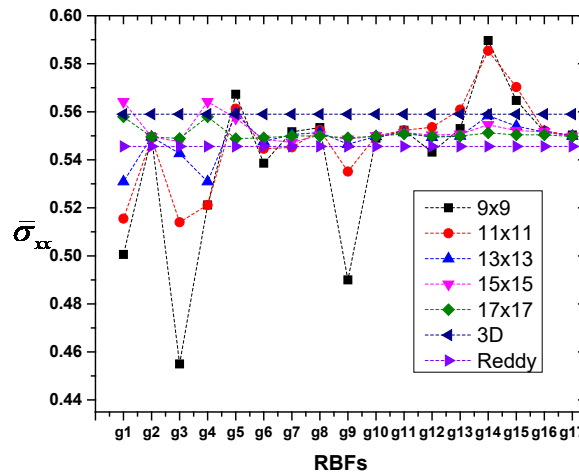
Fig. 3. Convergence study of $\bar{\sigma}_{xx}$ for (0/90/90/0) cross ply laminated plate (a/h=10) via seventeen RBFs
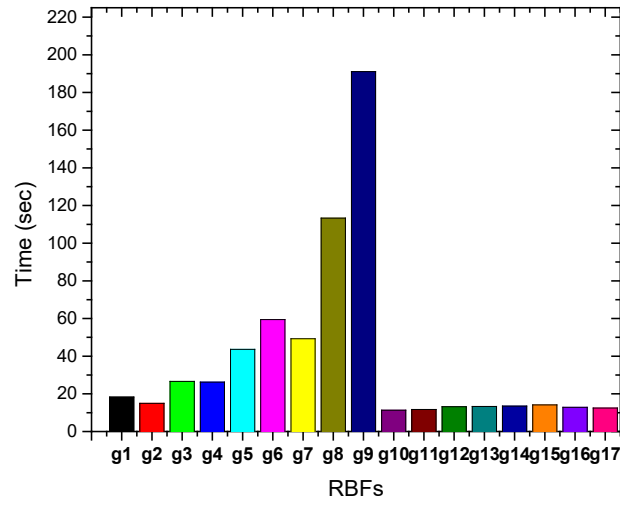
Fig. 4. Comparison study of central deflections with the computational speed of several RBFs.

4.2 Numerical examples

The analysis is further extended for a laminated plate subjected to I, L, T loading. Table 3 shows the influence of *I*, *L* and *T* type transverse loading on central deflection and stresses of cross play (0/90/90/0) and angle ply (0/90/0/90) laminated plate resting on elastic foundations. The plate aspect ratio, *a/h* = 20, $E_1 = 30 \times E_2$ and RBF g10 is considered in the present analysis. It is observed from the results that the *T* type transverse loading shows more central deflection and normal stresses followed by *I* and *L* type of loading for cross-ply as well as angle ply laminates, whereas the trend is different for shear stresses. The effect of foundation is also investigated for the cross-ply as well as angle-ply laminated plate. It is observed that the normalized deflection decreases monotonically along with the increasing K_w and K_s.

Table 3. Influences of transverse loading on normalized deflection and stresses of cross ply (0/90/90/0) elastically supported laminated plate.

(K_w, K_s)	Lamination Type	F_z	$\bar{w}_c$	$\bar{w}_m$	$\bar{\sigma}_{xx}$	$\bar{\sigma}_{yy}$	$\bar{\sigma}_{xy}$	$\bar{\sigma}_{yz}$	$\bar{\sigma}_{xz}$
(0,0)	Cross ply (0/90/90/0)	L	0.354	0.4102	0.3899	0.1244	0.0445	1.1107	0.1151
		I	0.6756	0.6756	0.7825	0.6611	0.0356	0.3681	0.6488
		T	0.8145	0.8145	0.9499	0.8362	0.0446	0.4641	0.8529
	Angle ply (0/90/0/90)	L	0.4035	0.4269	0.0217	0.0065	0.0288	0.6691	0.0655
		I	0.7142	0.7142	0.0428	0.0136	0.0389	0.253	0.9238
		T	0.8576	0.8576	0.0523	0.0165	0.0514	0.3163	1.2565
(10,0)	Cross ply (0/90/90/0)	L	0.3369	0.3956	0.3688	0.1128	0.0437	1.1039	0.1058
		I	0.6476	0.6476	0.7477	0.6405	0.0344	0.3648	0.6322
		T	0.7812	0.7812	0.9086	0.8116	0.0432	0.4604	0.8328
	Angle ply	L	0.3834	0.4074	0.0204	0.0061	0.0279	0.6633	0.0559

	(0/90/0/90)	I	0.6816	0.6816	0.0407	0.013	0.0375	0.2458	0.9049
		T	0.8189	0.8189	0.0498	0.0157	0.0497	0.3078	1.2331
(0,10)	Cross ply (0/90/90/0)	L	0.1775	0.2226	0.1781	0.0406	0.0296	0.8051	0.0341
		I	0.3623	0.3623	0.4012	0.3946	0.0217	0.3102	0.4351
		T	0.4398	0.4398	0.4934	0.5057	0.0277	0.4002	0.5842
	Angle ply (0/90/0/90)	L	0.1957	0.2204	0.0091	0.0027	0.0171	0.5278	0.0004
		I	0.3673	0.3673	0.0209	0.0069	0.0227	0.1757	0.6551
		T	0.4442	0.4442	0.026	0.0084	0.0315	0.2245	0.9001
(10,10)	Cross ply (0/90/90/0)	L	0.1726	0.2182	0.1721	0.0374	0.0294	0.8024	0.0316
		I	0.3541	0.3541	0.3912	0.3885	0.0213	0.3093	0.4301
		T	0.4302	0.4302	0.4815	0.4983	0.0273	0.3991	0.578
	Angle ply (0/90/0/90)	L	0.1902	0.2156	0.0088	0.0026	0.0168	0.5258	0.0018
		I	0.3585	0.3585	0.0203	0.0067	0.0223	0.1738	0.6496
		T	0.4337	0.4337	0.0254	0.0082	0.031	0.2222	0.8931
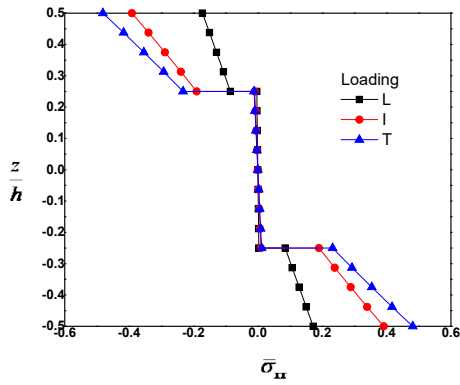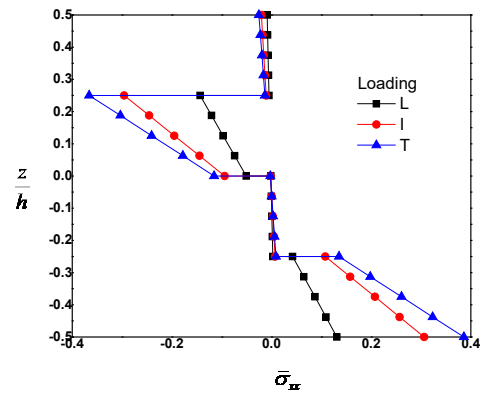
(a)   (b)

Fig. 5 Effect of transverse loading on $\bar{\sigma}_{xx}$ (a) cross ply (0/90/90/0) and (b) angle ply (0/90/0/90) laminated plate.
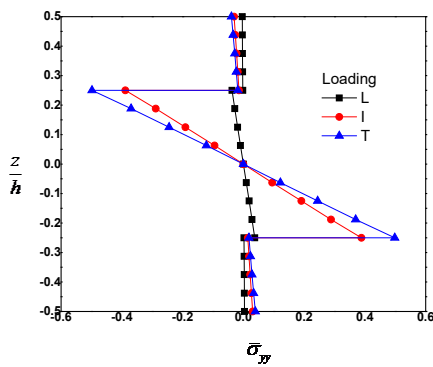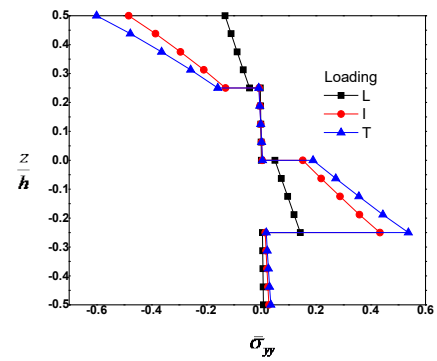
(a)   (b)

Fig. 6. Effect of transverse loading on $\bar{\sigma}_{yy}$ resting on (a) cross ply (0/90/90/0) and (b) angle ply (0/90/0/90) laminated plate.
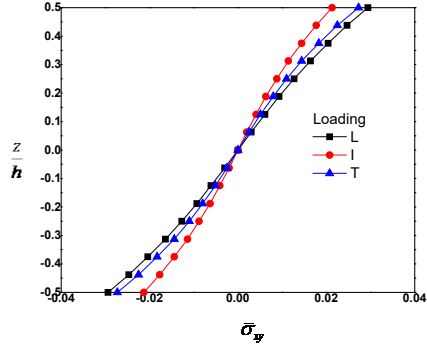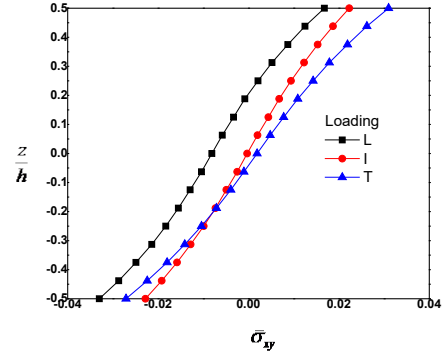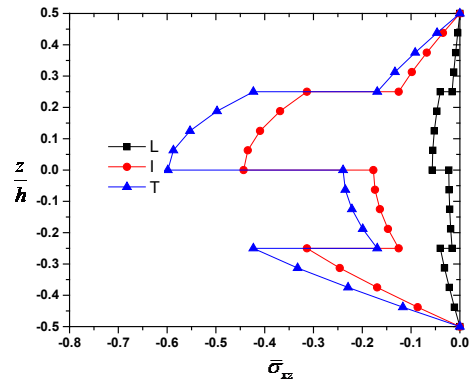
Fig. 7. Effect of transverse loading on $\bar{\sigma}_{xy}$ resting on (*a*) cross ply (0/90/90/0) and (*b*) angle ply (0/90/0/90) laminated plate.
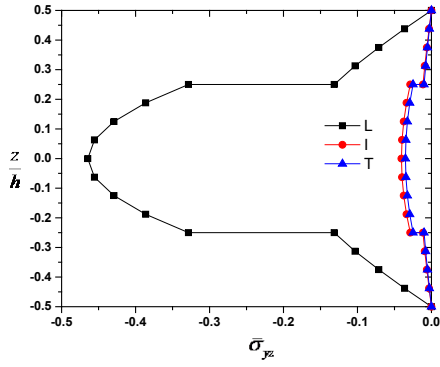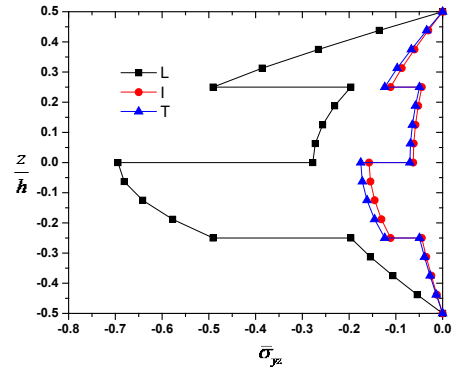
Fig. 8. Effect of transverse loading on $\bar{\sigma}_{yz}$ (*a*) cross ply (0/90/90/0) and (*b*) angle ply (0/90/0/90) laminated plate.
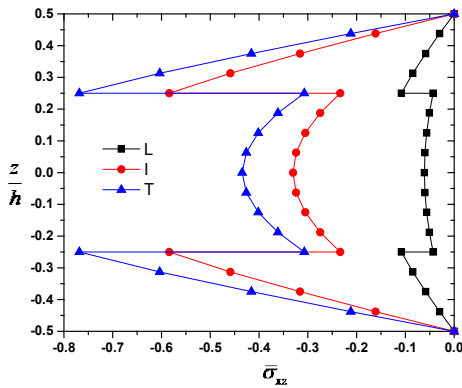
Fig. 9. Effect of transverse loading on $\bar{\sigma}_{xz}$ (*a*) cross ply (0/90/90/0) and (*b*) angle ply (0/90/0/90) laminated plate.

Figure 5 to 9 represent the effect of various types of loads on normal and shear stresses on cross ply (0/90/90/0) and angle ply (0/90/0/90) laminated plate (a/h=20, RBF = 10, h= 1/20, E_1=30 × E_2, K_w=10, K_s=10). Figures 5 and 6 represent through-the-thickness distributions of in plane normal stresses $\bar{\sigma}_{xx}$ and $\bar{\sigma}_{yy}$. Maximum normal stresses are produced by T load follow by I load and least by L load for cross ply and angle ply laminated plates. It is also observed that the value of $\bar{\sigma}_{xx}$ and $\bar{\sigma}_{yy}$ are zero at the z=0 mid-plane. Figure 7 represents the effect of I, L and T types of loading on $\bar{\sigma}_{xy}$ of cross ply (0/90/90/0) and angle ply (0/90/0/90) laminated plate. It is observed that the maximum value of $\bar{\sigma}_{xy}$ for angle ply and cross ply is generated on the boundary of the plate. Transverse shear stress through-the-thickness distributions for cross ply (0/90/90/0) and angle ply (0/90/0/90) laminated plate under I, L and T types of loading are depicted in Figure 8 and 9. From Figure 8, it is observed that the $\bar{\sigma}_{yz}$ get maximum value at $z = 0$ for cross ply and angle ply laminated plate and zero at top and bottom of the plate. From Figure 9, it is noticed that $\bar{\sigma}_{xz}$ is zero at top and bottom of the plate and follows the parabolic shape for all the three transverse shear stresses.
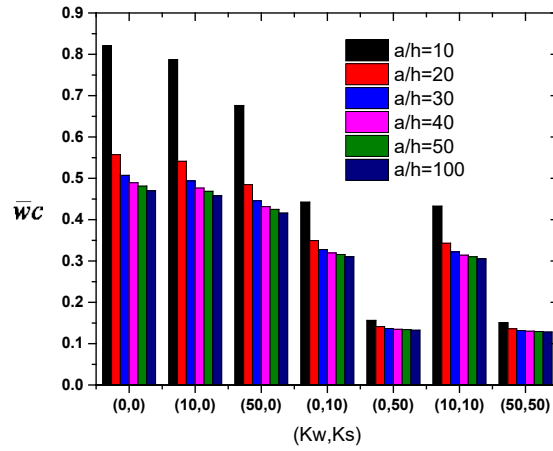
Fig. 10. Influences of a/h with elastic foundation on, $\bar{w}c$ for angle ply [45 -45 45 -45] laminated plate (g10, E_1=25 × E_2, Load type = T)

The normalized central deflection for angle ply [45 -45 45 -45] laminated plate subjected to T type load is computed for various a/h using g10 for various foundation parameters as shown in Figure 10. It is seen that by increasing the value of span to thickness ratio, $\bar{w}c$ starts decreasing and by increasing the value of K_w and Ks.
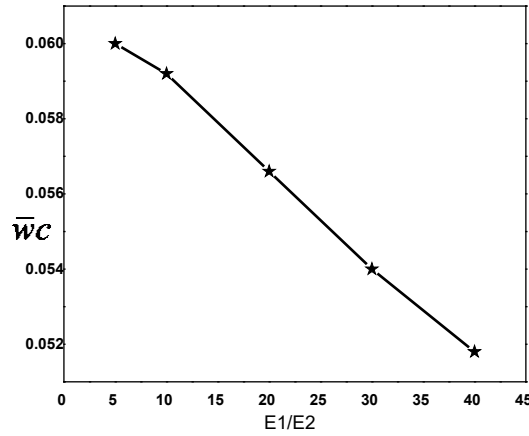
Fig. 11. Influences of orthotropic ratio (E_1/E_2) on central deflection, $\overline{w}c$ for angle ply [0 45 60 0] elastically supported laminated plate (g10, Load type= L, a/h=20, K_w=10, K_s=10)

Figure 11 shows the effect of orthotropic ratio vs elastic foundation for laminated plate. It is observed that by increasing the values of orthotropic ratio, the normalized deflection starts decreasing. Figure 12 represent the influences of elastic foundation on normal and shear stresses for angle ply [0 45 60 0] laminated plate. From Figure 12, it is observed that by increasing the values of K_w and K_s, the maximum stresses start decreasing for all the normal and shear stresses. Table 4 represent the 2D contours views on the influence of elastic foundation on normalized deflection under L, T, and I type transverse loading. It is observed that by increasing the values of K_w and K_s, normalized deflection starts decreasing.
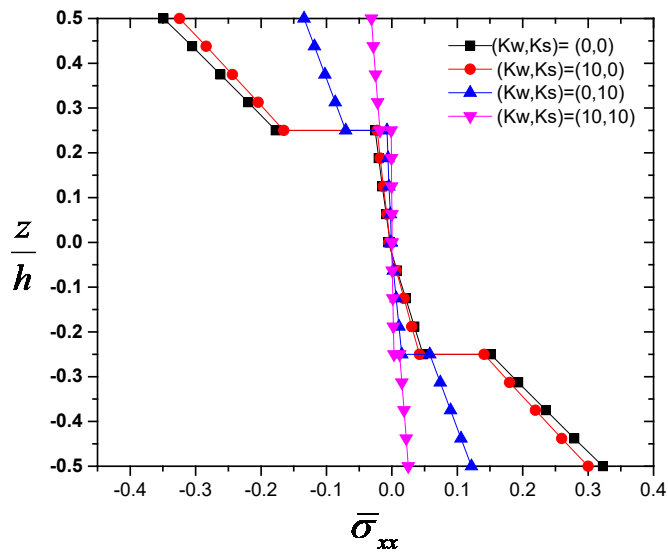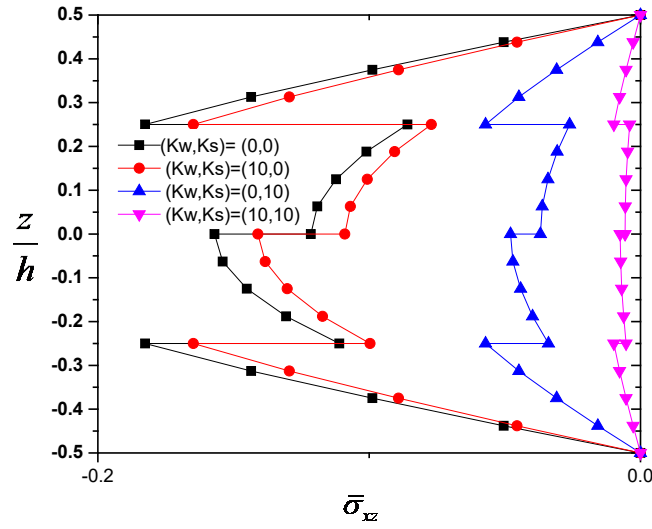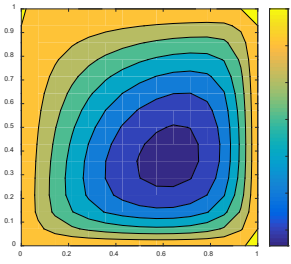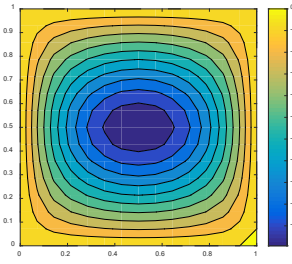

(a)
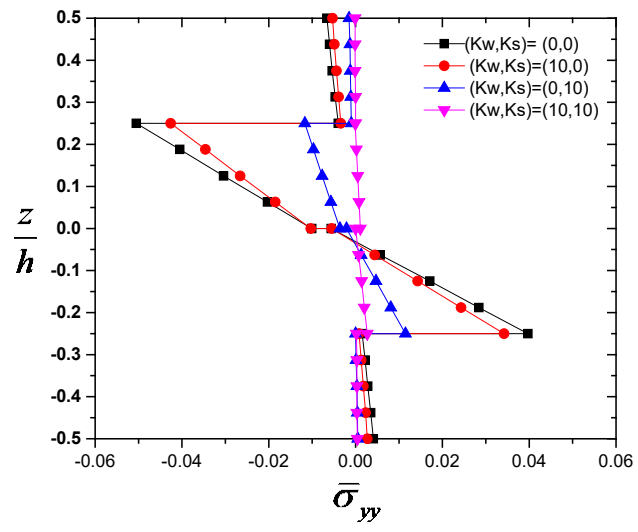
(b)
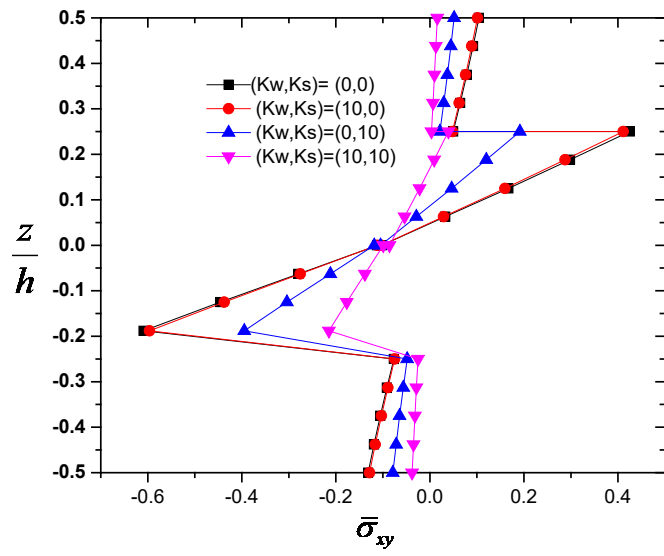
(c)
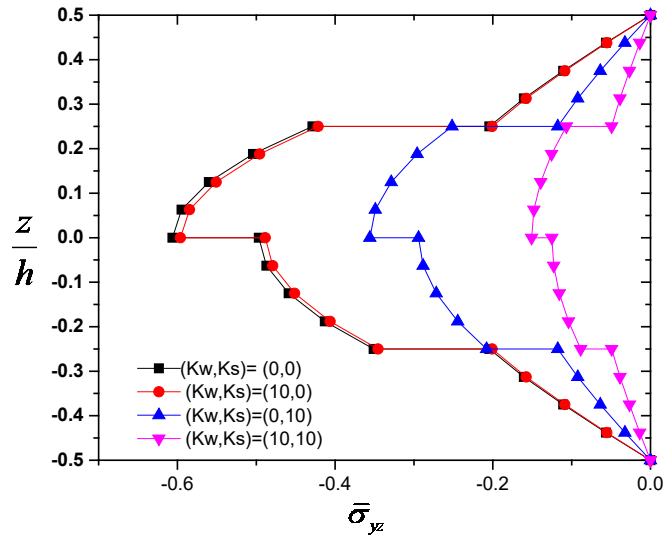
(d)
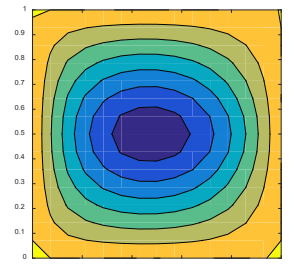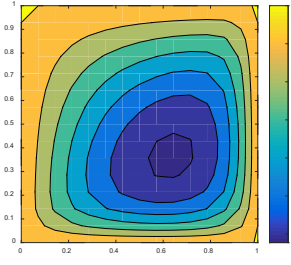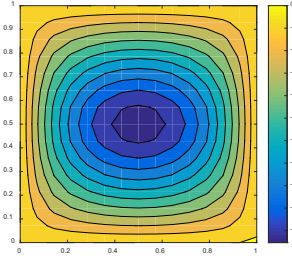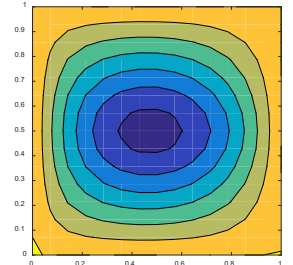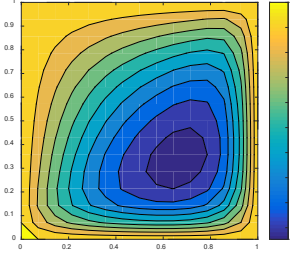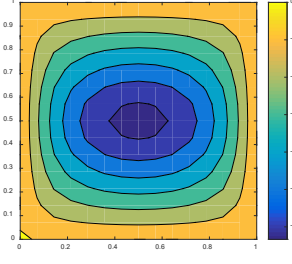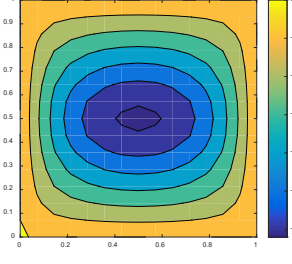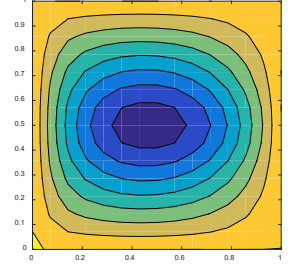
(e)

Fig. 12 Influences of elastic foundation (K_w, K_s) on normal (a) $\bar{\sigma}_{xx}$, (b) $\bar{\sigma}_{yy}$ and shear stresses (c) $\bar{\sigma}_{xy}$, (d) $\bar{\sigma}_{yz}$ and (e) $\bar{\sigma}_{xz}$ for angle ply [0 45 60 0] laminated plate through the thickness (g10, Load type= L, a/h=20, E_1/E_2 =20)
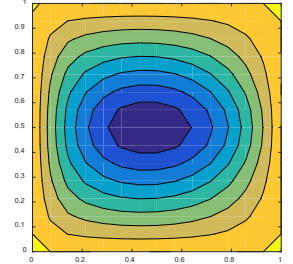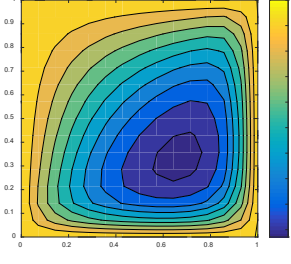
Table 4. The 2D contours representing the influence of elastic foundation on normalized central deflection $\bar{w}_c$ under different types of loading for angle ply [45 -45 45 -45] laminated plate. (g10, a/h=20, E_1/E_2 =20)

(K_w, K_s)	L-type	I-type	T-type

(0,0)			
	$\bar{w}_c = 0.2783$	$\bar{w}_c = 0.5460$	$\bar{w}_c = 0.6649$
	$\bar{w}_c = 0.2667$	$\bar{w}_c = 0.5266$	$\bar{w}_c$
	$\bar{w}_c = 0.1520$	$\bar{w}_c$	$\bar{w}_c$
(10,10)			
	$\bar{w}_c = 0.1481$	$\bar{w}_c = 0.3101$	$\bar{w}_c = 0.3803$

5. Conclusions

In the present study, elastically supported laminated plate's flexural analysis was carried out utilizing meshfree technique. The current displacement model was created using HSDT without the need for a shear correction factor. The governing equations were obtained using the Hamilton principle. Using RBFMCT, strong-formed solutions for the flexural analysis of elastically supported laminated plate with simple support were found. Bending behavior of elastically

supported laminated plate have been examined for a variety of factors, (Effect of transverse loading, effect of RBFs, span to thickness ratio, two variable elastic foundation, orthotropy ratio). The present results were verified and unambiguously demonstrated how quickly the existing simulation approach can determine displacements and stresses.

Based on the current results described in this paper, the following conclusions have been obtained:

- The present solution methodology is capable of finding the stresses and deflection under I, L and T transverse load.

- All the RBFs are a fast convergence rate with acceptable accuracy.

- The computational speed of RBFs g2, g10, g11, g12, g13, g14, g15, g16, and g17 is good as compared to other RBFs.

- The maximum deflection and stresses are minimum for L type of loading followed by I and T type of loading.

- The normalized deflection decreases by increasing the value of elastic foundation K_w and K_s.

- The normalized deflection decreases with an increase in E_1/E_2 ratio.

- The normalized deflection decreases with an increase in span to thickness ratio.

The research results and calculations presented in this paper are particularly remarkable because they advance our understanding of how this structure functions mechanically and help us assess, compute, and create mechanical models.

REFERENCES

[1]   Pagano NJ. Exact Solutions for Composite Laminates in Cylindrical Bending. Journal of Composite Materials, **3**, 398–411 (1969).
[2]   Pagano NJ. Exact Solutions for Rectangular Bidirectional Composites and Sandwich Plates. Journal of Composite Materials, **4**,20–34 (1970).
[3]   Srinivas S, Rao AK. Bending, vibration and buckling of simply supported thick orthotropic rectangular plates and laminates. International Journal of Solids and Structures, **6**,1463–81 (1970).
[4]   Reddy BS, Reddy AR, Kumar JS, Reddy KVK. Bending analysis of laminated composite plates using finite element method. International Journal of Engineering, Science and Technology,**4**,177–90 (2012).
[5]   Savithri S, Varadan TK. Accurate bending analysis of laminated orthotropic plates. AIAA Journal, **28**,1842–1854 (1990).
[6]   Sahoo SS, Panda SK, Singh VK. Experimental and numerical investigation of static and free vibration responses of woven glass/epoxy laminated composite plate. Proceedings of the Institution of Mechanical Engineers, Part L: Journal of Materials: Design and Applications,**231**,463–78 (2017).

[7] Karama M, Afaq KS, Mistou S. A new theory for laminated composite plates. Proceedings of the Institution of Mechanical Engineers, Part L: Journal of Materials: Design and Applications,**223**,53–62 (2009).

[8] Paydar N, Libove C. Bending of Sandwich Plates of Variable Thickness. Journal of Applied Mechanics,**55**,419–24 (1988)

[9] Saood A, Khan AH, Equbal MI, Saxena KK, Prakash C, Vatin NI, et al. Influence of Fiber Angle on Steady-State Response of Laminated Composite Rectangular Plates. Materials,**15**,5559 (2022).

[10] Khan A, Saxena KK. A review on enhancement of mechanical properties of fiber reinforcement polymer composite under different loading rates. Materials Today: Proceedings,**56**,2316–22 (2022).

[11] Rodrigues DES, Belinha J, Dinis LMJS, Natal Jorge RM. A meshless study of antisymmetric angle-ply laminates using high-order shear deformation theories. Composite Structures,**255,**112795 (2021).

[12] Chai GB, Yap CW, Lim TM. Bending and buckling of a generally laminated composite beam-column. Proceedings of the Institution of Mechanical Engineers, Part L: Journal of Materials: Design and Applications, **224**,1–7 (2010).

[13] Ferreira AJM, Castro LMS, Bertoluzza S. A high order collocation method for the static and vibration analysis of composite plates using a first-order theory. Composite Structures,**89**,424–32, (2009).

[14] Pavan GS, Nanjunda Rao KS. Bending analysis of laminated composite plates using isogeometric collocation method. Composite Structures;**176**, 715–28, (2017).

[15] Xiao JR, Gilhooley DF, Batra RC, Gillespie JW, McCarthy MA. Analysis of thick composite laminates using a higher-order shear and normal deformable plate theory (HOSNDPT) and a meshless method. Composites Part B: Engineering,**39**,414–27(2008).

[16] Ray MC. Three-dimensional exact elasticity solutions for antisymmetric angle-ply laminated composite plates. Int J Mech Mater Des., **17**,767–82 (2021).

[17] Sarra SA. Integrated multiquadric radial basis function approximation methods. Computers & Mathematics with Applications,**51**,1283–96 (2006).

[18] Multiquadric equations of topography and other irregular surfaces. Journal of Geophysical Research,**76**,1905–15, (1971).

[19] Kansa EJ. Multiquadrics—A scattered data approximation scheme with applications to computational fluid-dynamics—I surface approximations and partial derivative estimates. Computers & Mathematics with Applications,**19**,127–45(1990).

[20] Ferreira AJM, Roque CMC, Martins PALS. Radial basis functions and higher-order shear deformation theories in the analysis of laminated composite beams and plates. Composite Structures, 66,287–93 (2004).

[21] Ferreira AJM. A formulation of the multiquadric radial basis function method for the analysis of laminated composite plates. Composite Structures,**59**,385–92 (2003).

[22] Kumar R, Lal A, Singh BN, Singh J. Meshfree approach on buckling and free vibration analysis of porous FGM plate with proposed IHHSDT resting on the foundation. Curved and Layered Structures, **6**,192–211 (2019).

[23] Ferreira AJM, Carrera E, Cinefra M, Roque CMC. Analysis of laminated doubly-curved shells by a layerwise theory and radial basis functions collocation, accounting for through-the-thickness deformations. Comput Mech,48,13–25(2011).

[24] Solanki MK, Kumar R, Singh J. Flexure Analysis of Laminated Plates Using Multiquadratic RBF Based Meshfree Method. Int J Comput Methods, **15**, 1850049 (2017).

[25] Tornabene F, Fantuzzi N, Viola E, Ferreira AJM. Radial basis function method applied to doubly-curved laminated composite shells and panels with a General Higher-order Equivalent Single Layer formulation. Composites Part B: Engineering,**55**,642–59(2013).

[26] Xiang S, Kang GW. Meshless Solution of the Problem on the Static Behavior of Thin and Thick Laminated Composite Beams. Mech Compos Mater, **54**,89–98 (2018).

[27] Liew KM, Zhao X, Ferreira AJM. A review of meshless methods for laminated and functionally graded plates and shells. Composite Structures,**93**,2031–41(2011).

[28] Kumar R, Lal A, Singh BN, Singh J. New transverse shear deformation theory for bending analysis of FGM plate under patch load. Composite Structures,**208**,91–100(2019).

[29] Akavci SS. Analysis of Thick Laminated Composite Plates on an Elastic Foundation with the Use of Various Plate Theories. Mech Compos Mater , **41**,445–60 (2005).

[30] Benhenni MA, Adim B, Daouadji TH, Abbès B, Abbès F, Li Y, et al. A Comparison of Closed-Form and Finite-Element Solutions for the Free Vibration of Hybrid Cross-Ply Laminated Plates. Mech Compos Mater,**55**,181–94 (2019).

[31] Nedri K, El Meiche N, Tounsi A. Free Vibration Analysis of Laminated Composite Plates Resting on Elastic Foundations by Using a Refined Hyperbolic Shear Deformation Theory. Mech Compos Mater,**49**,629–640(2014).

[32] Singh J, Shukla KK. Nonlinear flexural analysis of laminated composite plates using RBF based meshless method. Composite Structures,**94,**1714–1720 (2012).

[33] Tran LV, Kim S-E. Static and free vibration analyses of multilayered plates by a higher-order shear and normal deformation theory and isogeometric analysis. Thin-Walled Structures,**130**,622–640 (2018).

[34] Reddy JN, Liu CF. A higher-order shear deformation theory of laminated elastic shells. International Journal of Engineering Science, **23**,319–30(1985).